Reconfigurable Parallel Plasmonic Transmission Lines With Nanometer Light Localization and Long Propagation Distance

Ran Hao, *Member, IEEE*, Eric Cassan, Yang Xu, *Member, IEEE*, Min Qiu, *Member, IEEE*, Xing-Chang Wei, *Senior Member, IEEE*, and Er-Ping Li, *Fellow, IEEE*

***Abstract*—A hybrid plasmonic parallel transmission line scheme constructed by a spatial single mode with time-domain multiline waveguide is presented in this paper. The proposed configuration enables a nanometer light localization while retaining a long propagation distance ($\sim$74 μm) at optical communication wavelengths with no crosstalk between data channels. High extinction ratio between the nanoribs peak energies ($\sim$20 dB) has been achieved after optimization. Furthermore, the proposed optical parallel transmission line scheme shows the advantages of enabling an optical device with a large number of parallel transmission channels, as well as a good robustness with respect to the fabrication tolerances.**

***Index Terms*—Data transmission, nanometer confinement, photonic integrated circuits, propagation distance, surface plasmon polaritons.**

I. Introduction

SURFACE plasmon polariton (SPP) structures are believed to be promising candidates for highly integrated nanophotonic circuits because of their unprecedented ability to concentrate light far beyond the diffraction limit [1]–[3]. The main bottleneck for SPP devices origins from the tradeoff between modal confinements and losses [4]. When the SPP modes downscale to nanometer sizes, huge losses occur and they propagate over limited distances [4], [5]. In this context, recent reported hybrid SPP structures (HSPP) [6]–[12] have attracted a great attention given that their propagation lengths extend fairly beyond than those of conventional SPPs [13]–[18] while maintaining small mode sizes at nanometer scale [19]. Various HSPP waveguides consisting of circle [6], trapezoid [20], or rectangular [21] shapes have been investigated, including complementary metal oxide semiconductor compatible structures [22]. Owing to the existence of high dielectric media, there are at least two advantages of HSPP configurations: they can improve the coupling efficiency by direct injection of light from a high dielectric media to metals [23], and they can reduce optical losses by using the high dielectrics as amplifying media [24], [25].

On the other hand, although HSPPs have several potential advantages, there is a demand to tune their plasmonic properties such as mode size, propagation distance, and modal index for the realization of functional active SPP components. The lack of tunability limiting the boom of HSPP-based functional devices.

In this paper, we discuss the realization of reconfigurable HSPPs and propose for this a parallel transmission line scheme for multichannel data transmission while maintaining the whole device in the nanometer scale, as well as a zero crosstalk propagation length up to 74 μm simultaneously. The presented results could help to improve the integration density on semioptical chips, showing promising prospects in future photonic functional components such as optical waveguides, switches, or modulators.

II. Cross-Index-Confined Mechanism

Naturally, SPPs allow strong coupling between electromagnetic waves and collective electron oscillations at a dielectric–metal interface. When a high-refractive index (silicon, $n_H = 3.5$) medium is approaching a metal surface in a low-index embedding dielectric (air, $n_L = 1$) background [e.g., with a triangular shape as shown in Fig. 1(a) or with a circle shape as shown in Fig. 1(b)], the SPP field distribution strongly varies with the gap size [6]. With smaller gap sizes, e.g., of a few nanometers, the field is vertically confined inside the gap but spreads through along the horizontal direction [6]. To squeeze the field horizontally, a small nanorib is deliberately located on the metal surface below the high-refractive index medium [see Fig. 1(a) and (b)]. The presence of this nanorib does not change the energy concentrated inside the gap, but drastically changes the electromagnetic field distribution along the metallic surface. The materials from bottom to top are arranged as a negative-index metal (silver), a low-index dielectrics, and high-index dielectrics. The materials from left to right are: low-index dielectrics, metal, and low-index dielectrics. Such arrangements

Manuscript received July 6, 2012; revised October 2, 2012, December 6, 2012, and December 31, 2012; accepted December 31, 2012. Date of publication January 4, 2013; date of current version April 25, 2013. This work was supported by the National Natural Science Foundation of China under Grant 61205054, the Zhejiang Provincial Natural Science Foundation of China under Grant Z1110330 and Grant LQ12F05006, the Fundamental Research Funds for the Central Universities, and the Excellent Young Faculty Awards Program (Zijin Plan) at Zhejiang University.

R. Hao, Y. Xu, X.-C. Wei, and E.-P. Li are with the Radio Frequency & Nano-Electronic Research Centre, Department of Information Science & Electronic Engineering, Zhejiang University, Hangzhou 310027, China (e-mail: rhao@zju.edu.cn; yangxu-isee@zju.edu.cn; weixc@zju.edu.cn; liep@zju.edu.cn).

E. Cassan is with the Institute of Fundamental Electronics, Université Paris Sud, Orsay 91400, France (e-mail: eric.cassan@u-psud.fr).

M. Qiu is with Department of Optical Engineering, Zhejiang University, Hangzhou 310027, Zhejiang, China (e-mail: minqiu@zju.edu.cn).

Color versions of one or more of the figures in this paper are available online at http://ieeexplore.ieee.org.

Digital Object Identifier 10.1109/JSTQE.2013.2237886

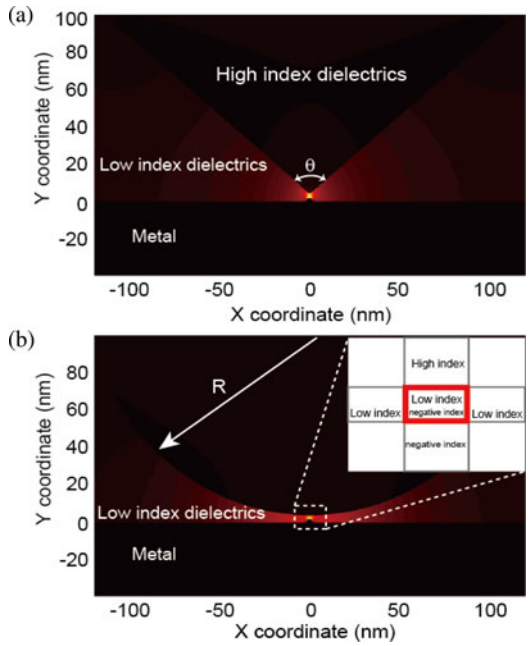

Fig. 1. Normalized electric field distributions for the fundamental mode in the two following geometries: (a) triangular-shape high-index dielectrics above a metallic nanorib characterized by $\theta = 100°$, and (b) fan-shaped high-index dielectrics above a metallic nanorib characterized by $R = 125$ nm. The considered permittivity for metal and high/low dielectrics are $-129 + 3.3i$ and 12.25/1 at the wavelength of 1550 nm, with $w_R = 10$ nm and $h_R = 2$ nm.

draw a cross-index variation inside the plane, providing strong field concentration at the center of the cross, as shown in the inset of Fig. 1(b). Therefore, light is vertically (Y direction) sandwiched in the gap between the high-index medium and the metallic substrate, and is horizontally (X direction) localized by the finite width w_R of a metallic convex rib, which be called, hereafter, a cross-index-confined SPP [26].

The geometries in Fig. 1 show strong field localizations but their fields are sensitive to the position of the nanorib. For instance, if the nanorib is slightly deviated from its original position or if there are more than one nanorib on the metallic surface, the strong field localization is affected because the cross-index geometry is changed. To ensure a better tolerance for the structural variation, a high-refractive index slab with an infinite width is appreciated, referring, for example, to the extreme cases $\theta = 180°$ in Fig. 1(a) or $R = \infty$ in Fig. 1(b). Once the width of the top slab becomes infinite, a subsequent question is: can the cross-index-confined mechanism still work well? In the vertical direction, the material arrangement still follows the rule: negative-index metal, low-index dielectrics, and high-index dielectrics. And so does in the horizontal direction. There is no strong change for the index arrangement both vertically and horizontally, as well as for the gap size. Hence, it is probable that the cross-index-confined SPP still exists at the center of the cross, even for this infinite-width-slab case. Fig. 2(a)–(c) shows the electromagnetic energy density distributions in this case. The energies are calculated using the commercial finite-element simulator COMSOL Multiphysics v4.2. It can be clearly seen that, as predicted, the optical energies are strong localized on the top area of the nanorib (at the center of geometrical cross) and that the energy rapidly decreases away from the center. The normalized electromagnetic energy densities [6] along two specified cutting lines [seen the inset pictures in Fig. 2(d) and (g)] are plotted. In the X direction, Fig. 2(d)–(f) shows the energy densities along the horizontal line, which is 1 nm above the top surface of the nanorib [seen the inset picture of Fig. 2(d)]. The fields reach their maximum values in the nanorib center, displaying a more or less Gaussian-like distribution. The calculated full-width at half-maximum (FWHM) values for considered cases are 16.9 nm [see Fig. 2(d)], 16.5 nm [see Fig. 2(e)], and 11.8 nm [see Fig. 2(f)], respectively. In the Y direction, Fig. 2(g)–(i) depicts the optical energy densities along the central vertical line [corresponding to $X = 0$ as seen in the inset of Fig. 2(g)]. The maximum values of the energy are always on the top surface of nanorib. The calculated FWHM values are 21.1 nm [see Fig. 2(g)], 10.1 nm [see Fig. 2(h)], and 2.3 nm [see Fig. 2(i)], respectively.

From these results, the influence of the nanorib height can also be estimated from the comparison between the three height values $h_R = 5$ nm [see Fig. 2(a), (d), and (g)], $h_R = 10$ nm [see Fig. 2(b), (e), and (h)], and $h_R = 18$ nm [see Fig. 2(c), (f), and (i)]. All the other geometrical parameters stay unchanged during the comparison. The strongest energy densities are obtained for the case $h_R = 18$ nm. As expected, the modification of nanorib height does not strongly affect the slope of the field distribution but more importantly changes its maximum density. The optical density is enhanced with a larger h_R value (due to a smaller gap size), but decreases when the h_R value becomes smaller (larger gap size).

III. Multichannel Configuration

There are at least two important observations derived from Fig. 2. First, the energy density is highly related to the gap size h_G and the nanorib height h_R. Modifying h_G and h_R can influence the optical energy directly. Second, the modifications of h_G and h_R still maintain the nanometer localization. Based on these two points, here we propose an application of the geometry studied in Section II to the design of plasmonic parallel transmission multilines proper to increase the agglomerated date rates. In Fig. 3, several nanoribs are inserted into the metallic substrate. The height above the substrate surface for each nanorib h_R or in other words the effective gap between each metallic nanorib and the high-index dielectrics is additionally supposed to be controlled by an efficient tuning mechanism. Among the possible solutions, the use of degenerate semiconductors as metal-like plasmonic materials dynamically filled with carriers using either electrical or optical electron/hole concentration modulations can be envisioned. We devote the following study to the analysis of the potentials of the proposed parallel plasmonic line concept in the hypothesis of such an efficient mechanism to individually modulate the effective gap sizes of the different nanoribs.

Fig. 3(a)–(c) shows the field distributions in the cross section under specified nanorib heights. The results exhibit that the optical energies are divided into high wave peaks and low wave peaks according to the different nanorib height, fitting the need for producing and transmitting semioptically—with

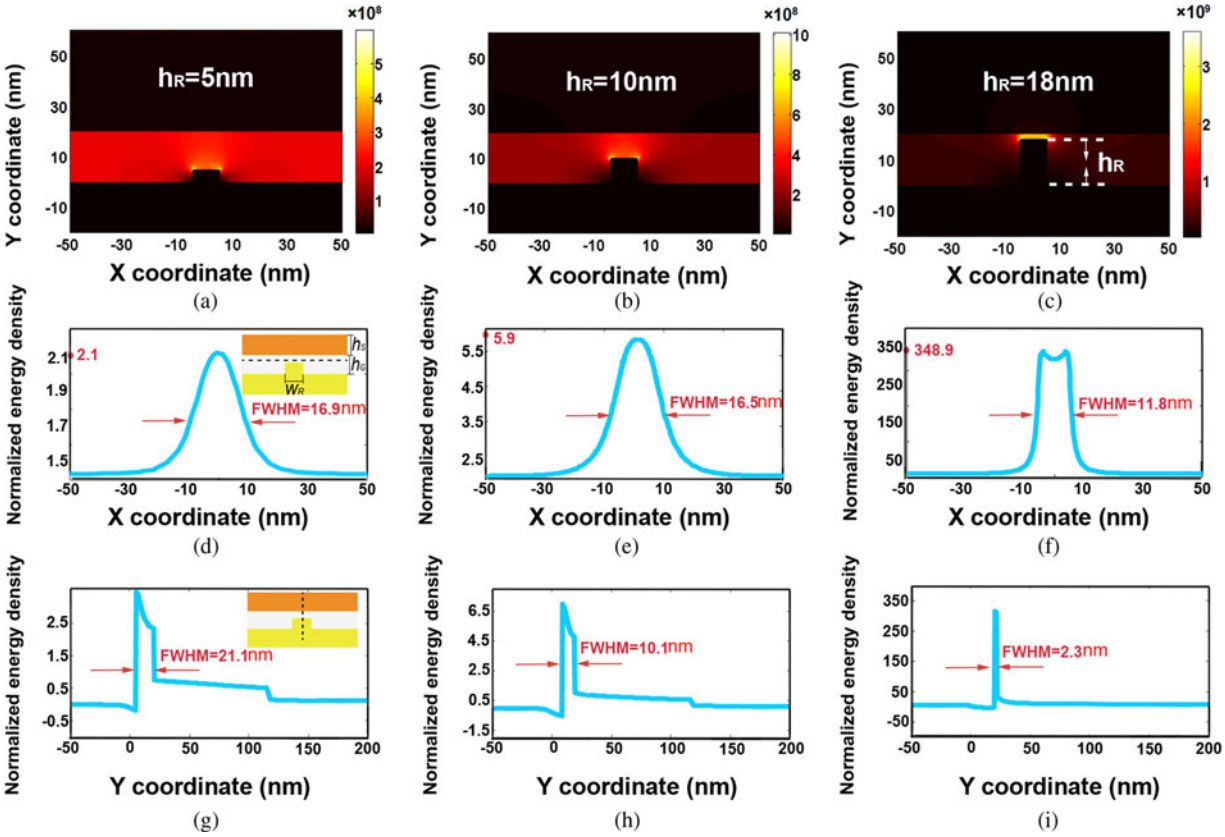

Fig. 2. Electromagnetic energy density distributions under the variation of h_R. (a)–(c) Normalized energy densities in the cross section for: (a) $h_R = 5$ nm, (b) $h_R = 10$ nm, (c) $h_R = 18$ nm. (d)–(f) Normalized energy densities distribution along the horizontal cutting line for: (d) $h_R = 5$ nm, (e) $h_R = 10$ nm, (f) $h_R = 18$ nm (the horizontal cutting line is 1 nm above the top surface of the nanorib, depicted in the inset of (d). (g)–(i) Normalized energy density distribution along the vertical cutting line under: (g) $h_R = 5$ nm, (h) $h_R = 10$ nm, (i) $h_R = 18$ nm (the vertical cutting line is in the center of the nanorib depicted in the inset of (g). In all the pictures, the thickness of the top slab h_S is 100 nm, the distance between the slab and the metal substrate h_G is fixed at 20 nm, and the width of nanorib w_R is 10 nm.

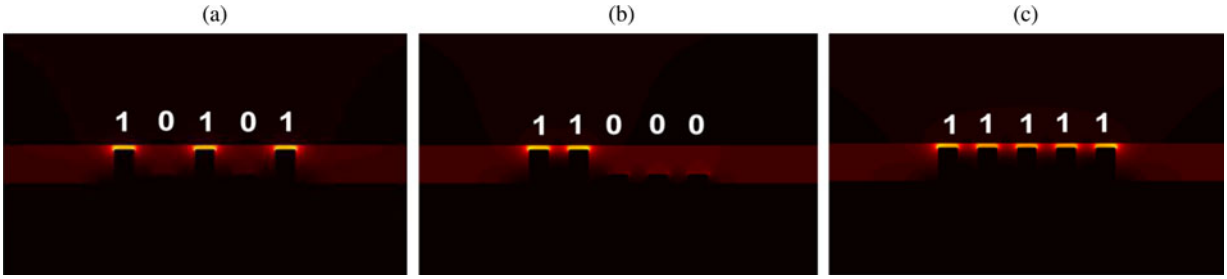

Fig. 3. Proposed optical parallel transmission lines scheme: normalized energy density distributions in the cross section under the control for three typical cases. (a) Information form of "10101" under $h_{R1} = 18$ nm, $h_{R2} = 5$ nm, $h_{R3} = 18$ nm, $h_{R4} = 5$ nm, $h_{R5} = 18$ nm. (b) Information form of "11000" under $h_{R1} = 18$ nm, $h_{R2} = 18$ nm, $h_{R3} = 5$ nm, $h_{R4} = 5$ nm, $h_{R5} = 5$ nm. (c) Information form of "11111" under $h_{R1} = 18$ nm, $h_{R2} = 18$ nm, $h_{R3} = 18$ nm, $h_{R4} = 18$ nm, $h_{R5} = 18$ nm. In all the pictures, the thickness of the top slab h_S is 100 nm, the distance between the top high-index medium and the metallic substrate is fixed at 20 nm, and the width of nanoribs w_R are all equal to 10 nm, the interval distance w_I is set to 20 nm.

modalities to be detailed later—"1" and "0" binary levels in the optical integrated circuits. In Fig. 3, we use "$h_R = 18$ nm" to produce high-energy peaks for signal "1," and "$h_R = 5$ nm" for signal "0." By modifying the height for each nanorib in the same device, the transferred information is "10101" in Fig. 3(a), "11000" in Fig. 3(b), and "11111" in Fig. 3(c). We shall point out that one big advantage of this parallel transmission lines is that the number of simultaneously transmitted signal channels can be extremely large owing to the available top slab width.

It should be emphasized here that we use energy peak or valley (portion of mode) to express the signal "1" and "0" above each nanorib, based on the fact that the modal distribution can be modified by changing the height of each nanoribs. Issues related to the possibility of transmitting several information channels by such a mechanism are further discussed in the next section.

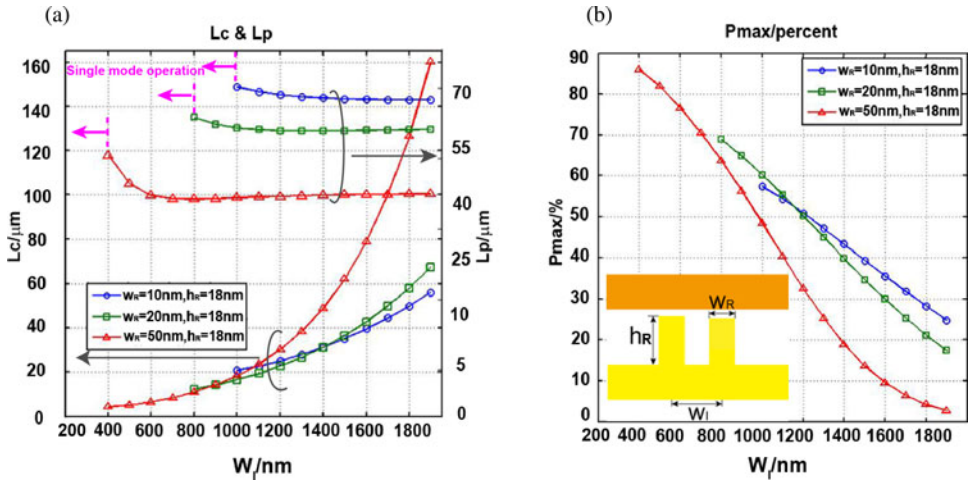

Fig. 4. (a) Influence of the interval distance w_I between two adjacent nanoribs on the coupling length and mean attenuation length of the whole propagating supermodes. (b) Influence of the interval distance w_I on the maximum transferred power $P_{\max}$. The distance between the top high-index medium and the metallic substrate is fixed at 20 nm.

IV. Signal Transmission

For any parallel multiwaveguide device, crosstalk between adjacent waveguides is a vital problem that influences the waveguide performances [27]. High crosstalk would cause serious signal distortion and information errors during the propagation. For conventional dielectric waveguides, the waveguide dimensions typically range from micrometers to some hundreds of nanometers, i.e., are typically comparable with light wavelength. This first point raises a limit to the photonic integration density. Additionally, when approaching parallel waveguides to make the circuit density increase, mode coupling makes crosstalk between waveguides unavoidable [28]–[30].

However, one advantage of the proposed parallel plasmonic transmission line scheme is that it is not based on the weak mode coupling between different waveguides. The nanorib mode dimension is indeed so small with respect to the light wavelength (e.g., the rib width $W_R = 10$ nm and the distance between two successive nanoribs is around $W_I = 20$ nm, while the wavelength is $\lambda = 1550$ nm) that their hybridization [6] with the top slab mode (comparable with λ) results in only one fundamental super-mode for the whole multichannel device. According to the performed numerical analysis calculations using both finite-element and finite-difference time-domain methods, only one even-symmetry hybrid mode (e.g., the fundamental mode of order 0) was indeed found at the working wavelength in all the explored configurations. As a result, the proposed parallel transmission lines work at single-mode operation and no crosstalk takes place when the device size is much smaller than wavelength.

To investigate how small the nanorib should be to allow the predicted working operation and, thus, estimate the constraints on the fabrication processes, we also studied the proposed waveguide configuration at larger dimensions. When the interval distance between adjacent nanoribs w_I increases to a certain value that is comparable with the wavelength, e.g., around $w_I = 1000$ nm, the odd mode (the first order) appears [as the blue circle line in Fig. 4(a)], then leading to a beating mechanism between the symmetric (even) and antisymmetric (odd) supermodes. Given the complex propagation constants $\beta_S + i\alpha_S$ and $\beta_a + i\alpha_a$ for the symmetric and antisymmetric modes, the coupling length L_C (the length within which the energy from one waveguide is coupled into the neighboring waveguide across the partition) is classically given as [30], [31]

$$L_C = \frac{\pi}{\beta_S - \beta_a}. \tag{1}$$

Similarly, the mean attenuation length L_P (the length representing the propagation loss, which is approximately twice of the propagation length for weak coupling) can be defined as [30], [31]

$$L_P = \frac{2}{\alpha_S + \alpha_S}. \tag{2}$$

Due to the existence of propagation losses, a total (100%) transfer of the electromagnetic energy from one waveguide to the other is not possible. The maximum power obtainable from one waveguide to the other due to coupling is then defined as [30], [31]

$$P_{\max} \cong \frac{\exp(-2\chi \arctan(1/\chi))}{1+\chi^2}, \chi = 2L_C/(\pi L_P). \tag{3}$$

Fig. 4 depicts the waveguide properties (L_C, L_P, and $P_{\max}$) of the multi-nano-rib plasmonic waveguide as a function of the W_I distance between two neighboring nanoribs under three sets of nanorib parameter (W_R H_R) combinations. It can be seen that with smaller w_R values, the range of W_I for single-mode operation becomes larger. Under $W_R = 10$ nm and $H_R = 18$ nm, the single-mode condition is W_I<1000 nm. In other words, there is no crosstalk due to the single supermode when W_I is scaled from nanometer dimensions up to 1μm contrary to nanowires for which the distance between two parallel nanowires typically need to be of several microns to achieve low crosstalk levels.

In the same time, the following question then arises: Now that the zero crosstalk operation is established due to the single-mode

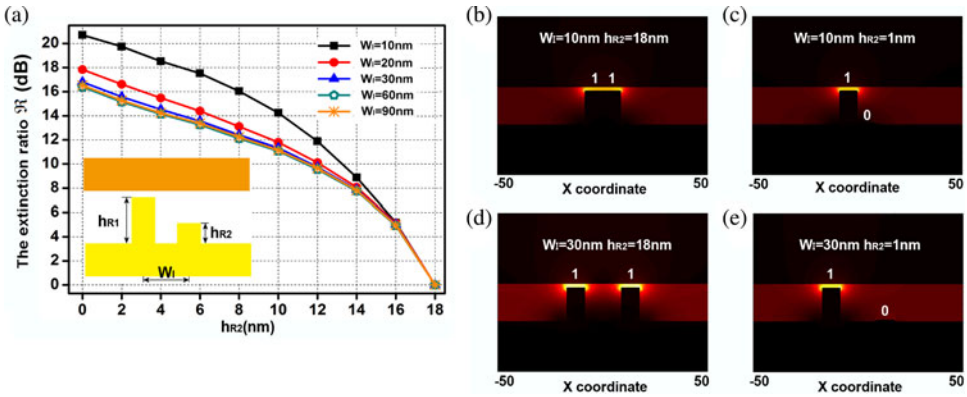

Fig. 5. (a) Extinction ratio performance for the proposed transmission lines, (b–e) Normalized electromagnetic field density distributions for: (b) $w_I = 10$ nm, $h_{R2} = 18$ nm, (c) $w_I = 10$ nm, $h_{R2} = 1$ nm, (d) $w_I = 30$ nm, $h_{R2} = 18$ nm, (e) $w_I = 30$ nm, $h_{R2} = 1$ nm, the other geometrical parameters are $w_R = 10$ nm, $h_{R2} = 18$ nm, and the slab thickness $h_G = 20$ nm.

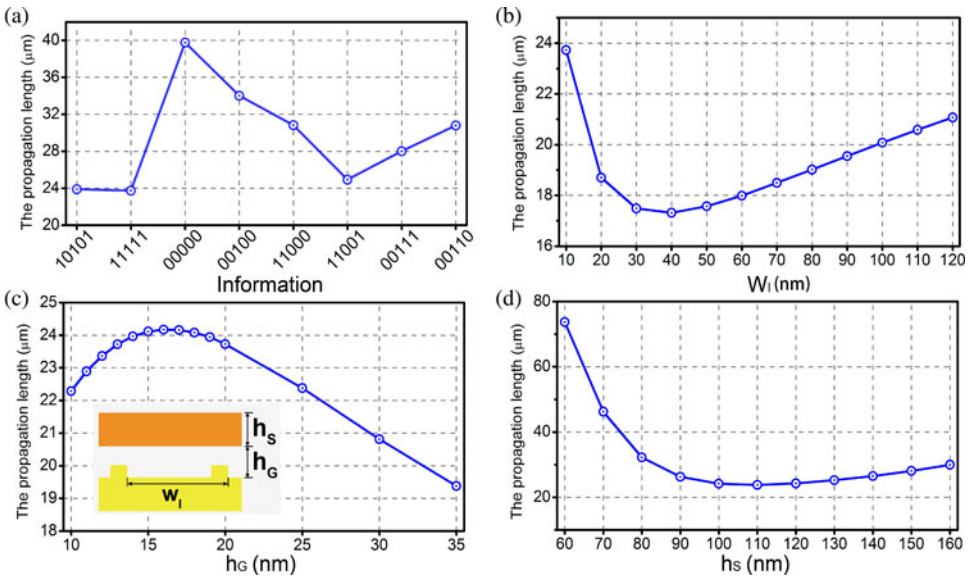

Fig. 6. (a) Propagation length under different information form. (b) Influence of w_I to the propagation length. (c) Influence of h_G on the propagation length. (d) Influence of h_S on the propagation length. The definitions of w_I, h_G, and h_S are depicted in the inset of (c). In all the pictures, the heights of convex are $h_{R1} = h_{R2} = h_{R3} = h_{R4} = h_{R5} = 18$ nm, and the widths of the nanoribs w_R are all 10 nm.

guiding mechanism, can it be said that the proposed multiple strong spots (one on each nanorib) configuration holds more than one information period or not?

First, obviously, the electromagnetic field visits all the nanogaps on top of the nanoribs or nothing, leading to the following consequence: for a given whole configuration of the nanorib gaps, the supermode field distribution is fixed and each individual nanogap cannot be modified without canceling the supermode field distribution itself. When transmitting a given list of digits, e.g., "10101" like in Fig. 4(a), all the effective gaps have, thus, to be maintained the same way to enable the transmission of the information from the initial time of encoding till the required time needed for the SPP wave to reach the set of detectors. Under this condition, and aligning a set of nanodetectors in front of the nanoribs to individually feel the high/low intensity levels corresponding to each of the low/strong spots, the list of digits made of a potentially large number of digits (the same as the number of nanoribs) can be transmitted despite there is only one single supermode in the multiline device. For such nanoscale peak/valley distribution, light detection is difficult, but can be achieved by additional procedures. With the recent developments of super-resolution/super-lens detection going far beyond the optical diffraction limit, one can distinguish light spots with a few nanometer interval distances [32]. Moreover, it is also possible to increase the interval distance w_I to better distribute the different spot sizes of adjacent nanoribs, which will make the detection much easier.

Last, we quantify here the main requirement raised by the condition of maintaining the single-mode multiline configuration during the transmission of one list of digits. For instance, considering a 30-μm-long plasmonic multilines (this value will be justified in Section VI), and taking $h_s = 85$ nm, $h_G = 16$ nm, $W_i = W_R = H_R = 10$ nm [these values are taken from Fig. 6(d)], the calculated light group velocity is around 1.27×10^8 m/s, meaning a time of flight of around 0.24 ps for transmission of information along the line. As a result,

modulating the whole configuration of the plasmonic effective gaps with a clock period above this value—corresponding to an electrical frequency up to 4.2 THz—allows satisfying the condition of supermode preservation.

V. Extinction Ratio Between Nanoribs

The next important issue is how to choose the interval distance w_I between adjacent nanoribs, since no crosstalk occurs for all w_I values smaller than 1000 nm. Here, we examine the extinction ratio expressing the quality of ON/OFF ratio (e.g., "1"/"0"). Quantitatively, the extinction ratio is obtained by the ratio between the transmitted energy density for signal "1" and signal "0" in decibel format between two neighboring nanoribs, which represents the quality of transmitted signals, defined as

$$\Re = 10 \lg \left(\frac{\max(D_1)}{\max(D_0)} \right)$$

where D_1 and D_0 are the electromagnetic energy densities associated with the "1" and "0" signals.

To rigorously study the extinction ratio $\Re$ of our proposed plasmonic multilines, the simplest situation, a two nanoribs geometry, is investigated here and the two related nanorib heights are chosen as following: h_{R1} is fixed at 18 nm, while sweeping the other one's height h_{R2}. Fig. 5(a) shows the calculated extinction ratio $\Re$ values when h_{R2} varies from 0 to 18 nm by steps of 2 nm. As expected, $\Re$ reaches its maximum when $h_{R2} = 0$ because the energy difference is also maximum in this case. Fig. 5(a) also compares the $\Re$ performances when the interval distance w_I varies. It is found that when $w_I = 10$ nm [which means that the two nanoribs are in touch with each other, as can been seen in Fig. 5(b) and (c)], $\Re$ is maximum. Fig. 5(c) depicts the "contact situation" when $w_{R2} = 1$ nm, the vertical surface of the left nanorib (which supports the Ex field component) has suppressed the field supported by the horizontal surface of the right nanorib (Ey field component). Therefore, the extinction ratio at this case is enhanced. We also show in Fig. 5(e) the case when two nanoribs are separated from each other by the distance $w_I = 30$ nm for comparison. It is seen that the electromagnetic field in Fig. 5(e) for signal "0" is stronger than that in Fig. 5(c).

In short summary, the so-called extinction ratio $\Re$ is the highest when the horizontal distance reaches its minimum ($w_I = 10$ nm, two nanoribs are then in contact), while the vertical distance reaches its maximum ($w_{R1} = 18$ nm and $w_{R2} = 0$). The highest $\Re$ is more than 20 dB. However, when w_I reaches its minimum, the detection of different nanospots is extremely difficult and required the highest resolution. In another word, the designs of our device need to consider some balance between a very good extinction ratio and an easy detection scheme.

VI. Propagation Properties

We address in this section the propagation loss issue, which is of primary importance to allow the possible exploitation of signals in the proposed plasmonic multiline scheme. The propagation loss is evaluated in terms of the propagation length, which relates to the length when optical energy decays by a factor of 1/e to its original value [6], [26]. To check the best capabilities, the criterion here is to consider the worst case: the minimum propagation length while operating dynamic tuning processes of individual nanorib gap sizes.

Obviously, the proposed parallel transmission line scheme has plenty of operation states corresponding to different information forms, as can be seen in Fig. 6(a). The obtained propagation lengths are between 23.9 and 39 μm. The minimum propagation length is obtained when signal "11111" is transmitted because the overall gap size is the smallest in this case.

Before starting, geometrical parameters for the optimization are reminded first. As depicted in the inset of Fig. 6(c), w_I is the internal distance between two adjacent ribs, h_G is the gap size between the top slab and bottom metal, and h_S is the thickness of the top slab. We have investigated one parameter variation while keeping others unchanged in each case. Fig. 6(b) shows the dependence between the propagation length and w_I. The propagation length is observed first to decrease and then increase almost linearly for $w_I > 50$ nm but with a different slope if compared with the low w_I range below 30 nm. The minimum propagation length value is obtained when w_I is 40 nm, before and after which the propagation length reaches maximum values at 10 and 120 nm (in the studied w_I range). w_I larger than 120 nm is not appreciated for high-density integration because the large internal distance at this case will increase the total device size. This is why w_S at 10 nm is chosen for the following optimization in Fig. 6(c) and (d). The compromised choice of the gap size h_G is a little bit more complicated. On one side, h_G needs to provide enough space for the tuning of the effective nanorib gaps. On the other side, h_G cannot be too large. Otherwise, higher order modes will appear inside the gap. Hence, we specified here the range of h_G between 10 and 35 nm in Fig. 6(c). The propagation length shows a gradual increase when h_G increases from 10 to 16 nm. After reaching its maximum value at 16 nm, the propagation length begins to decrease when h_G further increases. As a result, $h_G = 16$ nm was chosen here for the following optimization process step. Finally, the result of the scan of the top slab thickness influence is shown in Fig. 6(d). When h_S is continuously increased from 60 to 160 nm, the propagation length is observed first to decrease from 73.7 to 23.8 μm, and then slowly increase to 30 μm. The conclusion is that smaller h_S will have larger propagation length. The propagation length for h_S larger than 160 nm was not investigated because larger h_S will cause the disappearance of hybrid SPP mode inside the gap (the exploited mode then begins to concentrate in the top silicon slab [6]). The obtained results indicate that h_S plays a key role for the propagation length of the system. A decrease of h_S results in an increase of the propagation length. In short summary, optimized results as follows have been obtained: $w_I = 10$ nm, $h_G = 16$ nm, and $h_S = 60$ nm to have a propagation length of around 74 μm with an ultracompact device size.

In the same time, these results can be correlated with the estimation of the overall plasmonic multiline mode size. The mode size issue has in fact already been studied in Fig. 2, exhibiting nanometer scale light localization above each nanorib. However, it can be seen that in Fig. 2, some portion of the light energy has flowed in the background (low-index region). This result, which

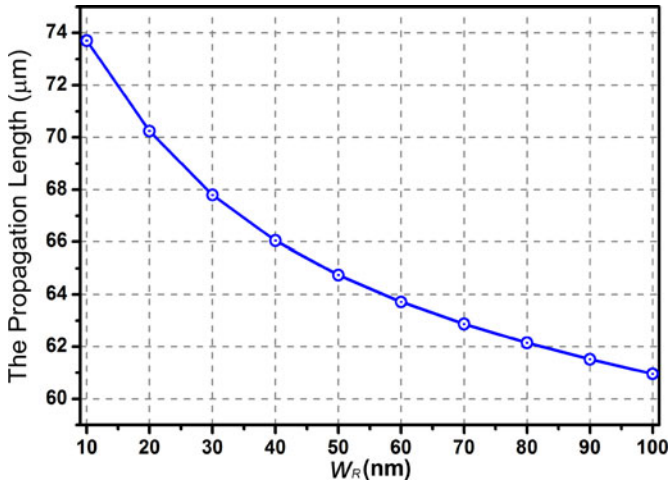

Fig. 7. Influence of nanorib width w_R on the propagation length.

is expected because the light wavelength is more than 150 times larger than the localization area, is accounted in the calculation of the propagation losses performed just above and is not an additional penalty. As part of the propagation mode, the weak energy in the background will propagate together with the central high-intensity field. There are two consequences: first, the existence of the background field has enlarged the overall mode size of the device, so the overall propagation length has been greatly extended. Second, it can achieve a large overall mode size but simultaneously a nanometer local field concentration at the center of index cross, which is the main important point here.

We choose the size of the nanorib $w_R = 10$ nm according to the best capability of the present clean room technology. An important advantage of the proposed parallel plasmonic multilines is that it is scale free with the geometrical dimensions (nonstrongly sensitive to the w_R value). At larger w_R values, the proposed parallel waveguides still work well. This is because the cross-index-confined mechanism together with the tuning mechanism is nonstrongly sensitive to w_R. In the same time, enlarging the geometrical dimension will have a small influence on the propagation properties. Fig. 7 depicts the influence of the w_R variation on the propagation length. The propagation length is observed to decrease with the increase of w_R but remains above 60 μm when enlarging w_R up to 100 nm.

This means that we do not have to approach the limits of fabricating technologies to already have fairly large propagation lengths.

VII. Conclusion

In conclusion, a plasmonic waveguide has been investigated for parallel transmission of multibit signals with the advantages of a potentially large number of information channels, zero crosstalk between adjacent channels, high extinction ratio, nanoscale light localization, as well as long propagation length. The exploited cross-index-confined mechanism ensures the possibility to include additional channels while the single-mode operation of the whole device at $\lambda = 1550$ nm is responsible for the investigated properties. Wide scans of the geometrical parameters have been numerically performed, showing that the extinction ratio can be as high as ~ 20 dB after optimization. Similarly, a propagation length as long as $\sim$74 μm is obtained simultaneously with a nanometer mode localization and ultracompact device size. The obtained results may help to enhance the integration density of semioptical chips, and hold significant future promises for developing components at nanometer scale for future semioptical integrated circuits and on-chips merging optics and nanoelectronics. Future works will be focused on the investigation of the possible tuning mechanisms to individually modify the effective gaps of the proposed nanorib configuration.

Acknowledgment

R. Hao would like to acknowledge H.-K. Yu in the Department of Optical Engineering, Zhejiang University, for the helpful discussions on the coupled mode theory. The authors would like to thank the assistance from J.-M. Jin, L.-F. Wang, L.-S. Cai, J. Wei, and W. Du in the Radio Frequency & Nano-Electronic Research Centre, Department of Information Science & Electronic Engineering, Zhejiang University.

References

[1] H. Raether, *Surface Plamons on Smooth and Rough Surface and on Gratings*. Ch. 2, New York: Springer, 1998.
[2] S. A. Maier and H. A. Atwater, "Plasmonics: Localization and guiding of electromagnetic energy in metal/dielectric structures," *J. Appl. Phys.*, vol. 98, pp. 011101-1–011101-10, 2005.
[3] J. A. Schuller, E. S. Barnard, W. S. Cai, Y. C. Jun, J. S. White, and M. S. Brongersma, "Plasmonics for extreme light concentration and manipulation," *Nat. Mater.*, vol. 9, pp. 193–204, 2010.
[4] D. K. Gramotnev and S. I. Bozhevolnyi, "Plasmonics beyond the diffraction limit," *Nat. Photon.*, vol. 4, pp. 83–91, 2010.
[5] T. W. Ebbesen, C. Genet, and S. I. Bozhevolnyi, "Surface-plasmon circuitry," *Phys. Today*, vol. 61, pp. 44–50, 2008.
[6] R. F. Oulton, V. J. Sorger, D. A. Genov, D. F. P. Pile, and X. Zhang, "A hybrid plasmonic waveguide for subwavelength confinement and long-range propagation," *Nat. Photon.*, vol. 2, pp. 496–500, 2008.
[7] R. Salvador, A. Martinez, C. Garcia-Meca, R. Ortuno, and J. Marti, "Analysis of hybrid dielectric plasmonic waveguides," *IEEE J. Sel. Topics Quantum Electron.*, vol. 14, no. 6, pp. 1496–1501, Nov./Dec. 2008.
[8] H. Benisty and M. Besbes, "Plasmonic inverse rib waveguiding for tight confinement and smooth interface definition," *J. Appl. Phys.*, vol. 108, pp. 063108-1–063108-8, 2010.
[9] D. X. Dai, Y. C. Shi, S. L. He, L. Wosinski, and L. Thylen, "Silicon hybrid plasmonic submicron-donut resonator with pure dielectric access waveguides," *Opt. Exp.*, vol. 19, pp. 23671–23682, 2012.
[10] D. X. Dai and S. L. He, "Low-loss hybrid plasmonic waveguide with double low-index nano-slots," *Opt. Exp.*, vol. 18, pp. 17958–17966, 2010.
[11] L. Chen, X. Li, G. P. Wang, W. Li, S. H. Chen, L. Xiao, and D. S. Gao, "A silicon-based 3-D hybrid long-range plasmonic waveguide for nanophotonic integration," *J. Lightw. Technol.*, vol. 30, pp. 163–168, 2012.
[12] H. Benisty and M. Besbes, "Confinement and optical properties of the plasmonic inverse-rib waveguide," *J. Opt. Soc. Amer. B*, vol. 29, pp. 818–825, 2012.
[13] E. Moreno, F. J. Garcia-Vidal, S. G. Rodrigo, L. Martin-Moreno, and S. I. Bozhevolnyi, "Channel plasmon-polaritons: Modal shape, dispersion, and losses," *Opt. Lett.*, vol. 31, pp. 3447–3449, 2006.
[14] D. F. P. Pile and D. K. Gramotnev, "Channel plasmon-polariton in a triangular groove on a metal surface," *Opt. Lett.*, vol. 29, pp. 1069–1071, 2004.
[15] S. I. Bozhevolyni, V. S. Volkov, E. Devaux, and T. W. Ebbesen, "Channel plasmon-polariton guiding by subwavelength metal grooves," *Phys. Rev. Lett.*, vol. 95, pp. 046802-1–046802-4, 2005.

[16] G. Veronis and S. H. Fan, "Guided subwavelength plasmonic mode supported by a slot in a thin metal film," *Opt. Lett.*, vol. 30, pp. 3359–3361, 2005.
[17] E. Moreno, S. G. Rodrigo, S. I. Bozhevolnyi, L. Martin-Moreno, and F. J. Garcia-Vidal, "Guiding and focusing of electromagnetic fields with wedge plasmon polaritons," *Phys. Rev. Lett.*, vol. 100, pp. 023901-1–023901-4, 2008.
[18] M. I. Stochman, "Nanofocusing of optical energy in tapered plasmonic waveguides," *Phys. Rev. Lett.*, vol. 93, pp. 137404-1–137404-4, 2004.
[19] M. Fujii, J. Leuthold, and W. Freude, "Dispersion relation and loss of subwavelength confined mode of metal-dielectric-gap optical waveguides," *IEEE Photon. Tech. Lett.*, vol. 21, no. 6, pp. 362–365, Mar. 2009.
[20] J. T. Kim and S. E. Choi, "Hybrid plamonic slot waveguides with sidewall slope," *IEEE Photon. Tech. Lett.*, vol. 24, no. 3, pp. 170–172, Feb. 2012.
[21] F. F. Lu, T. Li, X. P. Hu, Q. Q. Cheng, S. N. Zhu, and Y. Y. Zhu, "Efficient second-harmonic generation in nonlinear plasmonic waveguide," *Opt. Lett.*, vol. 36, pp. 3371–3373, 2011.
[22] D. X. Dai and S. L. He, "A silicon-based hybrid plasmonic waveguide with a metal cap for a nano-scale light confinement," *Opt. Exp.*, vol. 17, pp. 16646–16653, 2009.
[23] J. Tian, Z. Ma, Q. Li, Y. Song, H. H. Liu, Q. Yang, C. L. Zha, J. Akerman, L. M. Tong, and M. Qiu, "Nanowaveguides and couplers based on hybrid plasmonic modes," *Appl. Phys. Lett.*, vol. 97, pp. 231121-1–231121-3, 2010.
[24] J. Zhang, L. K. Cai, W. L. Bai, Y. Xu, and G. F. Song, "Hybrid plasmonic waveguide with gain medium for lossless propagation with nanoscale confinement," *Opt. Lett.*, vol. 36, pp. 2312–2314, 2011.
[25] D. X. Dai, Y. C. Shi, S. L. He, L. Wosinski, and L. Thylen, "Gain enhancement in a hybrid plasmonic nanowaveguide with a low-index or high-index gain medium," *Opt. Exp.*, vol. 19, pp. 12925–12936, 2011.
[26] R. Hao, E. P. Li, and X. C. Wei, "Two-dimensional light confinement in cross-index-modulation plasmonic waveguides," *Opt. Lett.*, vol. 37, no. 14, pp. 2934–2936, 2012.
[27] A. Hardy and W. Streifer, "Coupled mode theory of parallel waveguides," *J. Lightw. Technol.*, vol. LT-3, no. 5, pp. 1135–1146, 1985.
[28] H. A. Haus, W. P. Huang, S. Kawakami, and N. A. Whitaker, "Coupled-mode theory of optical waveguides," *J. Lightw. Technol.*, vol. LT-3, no. 1, pp. 16–23, 1987.
[29] W. P. Huang, "Coupled-mode theory for optical waveguides: An overview," *J. Opt. Soc. Amer. A*, vol. 11, pp. 963–983, 1994.
[30] G. Veronis and S. H. Fan, "Crosstalk between three-dimensional plasmonic slot waveguides," *Opt. Exp.*, vol. 16, pp. 2129–2140, 2008.
[31] Y. Song, M. Yan, Q. Yang, L. M. Tong, and M. Qiu, "Reducing crosstalk between nanowire-based hybrid plasmonic waveguides," *Optic. Commun.*, vol. 284, pp. 480–484, 2011.
[32] J. Wang, Y. Xu, H. Chen, and B. Zhang, "Ultraviolet dielectric hyperlens with layered graphene and boron nitride," *J. Mater. Chem.*, vol. 22, pp. 15863–15868, 2012.

Ran Hao (M'11) received the Ph.D. degree in physics from University Paris XI, Orsay, France, in December, 2010, and the second Ph.D. degree in photonics from Wuhan National Laboratory for Optoelectronics, Huazhong University of Science & Technology, Optical valley of China, Wuhan, China, in 2011.

He is currently an Assistant Professor with the Department of Information Science & Electronic Engineering, Zhejiang University, Hangzhou, China. His current research interests include nanoplasmonics, nanophotonics, nanofabrication, photonic crystals, slow light phenomena, and graphene photonics.

Dr. Hao is a member of the Optical Society of America. He received the Distinguished Young Scholar award in 2011 and the Excellent Young Faculty Awards Program (Zijin Plan) in 2012 at Zhejiang University.

Eric Cassan received the Ph.D. degree in physics from the Paris-Sud University, Orsay, France, in 2000 and the professor degree of the Paris-Sud University, Orsay, France, in 2009.

He is currently with the Institute of Fundamental Electronics, Université Paris Sud, Orsay, France. Since 2000, he has contributed to several French and European projects on on-chip optical interconnect based on the integration of all-silicon passive and active optical devices. His research interests include slow wave effects in photonic crystals, nonlinear effects in strongly confined photonic structures, and passive/active plasmonic structures.

Yang Xu (S'05–M'09) received the B.S. degree in electrical and computer engineering from Tsinghua University, Beijing, China, and the M.S. and Ph.D. degrees in electrical and computer engineering from the University of Illinois at Urbana and Champaign, Champaign.

He is currently an Associate Professor with the Department of Information Science & Electronic Engineering, Zhejiang University, Hangzhou, China. His research interests include exploring the theory, simulation, and fabrication of micro-/nanoelectronic devices.

Min Qiu (A'99–M'02) received the B.Sc. and Ph.D. degrees in condense matter physics from the Zhejiang University, Hangzhou, China, in 1995 and 1999, respectively, and the second Ph.D. degree in electromagnetic theory from the Royal Institute of Technology (KTH), Stockholm, Sweden, in 2001.

In 2001, he joined the School of Information and Communication Technology, KTH, as an Assistant Professor, and became an Associate Professor in 2005 and a Full Professor (Professor of photonics) in 2009. In 2010, he also became a Special-Term Distinguished Professor at the Zhejiang University. He is an author or coauthor of more than 140 international refereed journal papers, and more than 100 conference contributions, including more than 40 invited talks in international conferences. He has an h-index of 33 up to December 2012. His research interests include nanofabrication method, optical metamaterials, photonic crystals, plasmonic optics, and integrated optical circuits.

Dr. Qiu is a member of the Optical Society of America and the European Optical Society. He received the Individual Grants for the Advancement of Research Leaders (INGVAR) from the Swedish Foundation for Strategic Research (SSF) in 2004. He received the Senior Researcher Fellowship from Swedish Research Council.

Xing-Chang Wei (M'01–SM'09) received the Ph.D. degree in electrical engineering from Xi'an University of Electronic Science and Technology, Chengdu, China, in 2001.

From 2001 to 2010, he was with the ASTAR Institute of High Performance Computing, Singapore, as a Research Fellow, Senior Research Engineer, and then a Research Scientist. He joined Zhejiang University, Hangzhou, China as a Full Professor in 2010. He authored more than 40 papers published in prestigious international journals and conferences. He was the Co-Chair of technical program committee of 2010 IEEE electrical design of advanced packaging and systems symposium. His main research interests include 3-D IC analysis, power integrity and signal integrity simulation and design, EMC modeling and simulation, and the development of fast algorithms for computational electromagnetics.

Dr. Wei received the 2007 Singapore IES (Institution of Engineers) Prestigious Engineering Achievement Award for his contribution on the development of a novel electromagnetic compatibility simulation facility.

Er-Ping Li (S'91–M'92–SM'01–F'08) received the Ph.D. degree in electrical engineering from Sheffield Hallam University, Sheffield, U.K., in 1992.

From 1989 to 1992, he was a Research Associate/Fellow with the School of Electronic and Information Technology, Sheffield Hallam University. Between 1993 and 1999, he was a Senior Research Fellow, Principal Research Engineer, Associate Professor, and the Technical Director with the Singapore Research Institute and Industry. In 2000, he joined the Singapore National Research Institute of High Performance Computing as a Senior Scientist and the Head of the Lab, of Electromagnetics, and then became the Principal Scientist and the Director of the Electronic and Photonics Department. From 2010, he holds the appointment of Distinguished Professor in the Department of Information Science & Electronic Engineering, Zhejiang University, Hangzhou, China. He was the Guest Professor of Xi'an Jiaotong University and Peking University in China, an External Academy Advisor for the City University of Hong Kong, and a Global Advisor to Korea Advance Institute of Technology. He authored or coauthored more than 300 papers published in the referred international journals and conferences. He holds and has filed a number of patents at the U.S. patent office. His research interests include electrical modeling and design of micro/nanoscale integrated circuits, 3-D electronic package integration, and nanoplasmonic technology. He is pioneering in electrical modeling and design of advanced package integration and nanoplasmonic for nanoelectronics.

Dr. Li served as the Associate Editor for IEEE MICROWAVE AND WIRELESS COMPONENTS LETTERS from 2006 to 2008 and served the Guest Editor for 2006 and 2010 IEEE TRANSACTIONS ON ELECTROMAGNETIC COMPATIBILITY special issues, Guest Editor for 2010 IEEE TRANSACTIONS ON MICROWAVE THEORY AND APPLICATIONS APMC special issue. He is currently the Associate Editor for IEEE TRANSACTIONS ON ELECTROMAGNETIC COMPATIBILITY and IEEE TRANSACTIONS ON COMPONENTS AND PACKAGING TECHNOLOGIES. He is the Founding Member of the IEEE Machine Tool Technologies Research Foundation Nanotechnology Committee. He has been a General Chair and Technical Chair for many international conferences. He was the President for 2006 International Zurich Symposium on EMC, the General Chair for the 2008, 2010, and 2012 Asia-Pacific EMC Symposium, General Chair for 2010 IEEE Symposium on Electrical Design for Advanced Packaging Systems, and the Chairman of the IEEE EMC Singapore Chapter for 2005–2006. He has been invited to give numerous invited talks and plenary speeches at various international conferences and forums. He is a fellow of the MIT Electromagnetics Academy, USA. He received the IEEE EMC Technical Achievement Award, Singapore IES Prestigious Engineering Achievement Award, and Changjiang Chair Professorship Award from the Ministry of Education in China, and number of Best Paper Awards. He was elected to the IEEE EMC Distinguished Lecturer in 2007.